1-1-2014

Mixed quadratic-cubic autocatalytic reaction-diffusion equations: Semi-analytical solutions

Muteb Alharthi
University of Wollongong, mraah761@uowmail.edu.au

Timothy Marchant
University of Wollongong, tim@uow.edu.au

Mark Nelson
University of Wollongong, mnelson@uow.edu.au

Mixed quadratic-cubic autocatalytic reaction-diffusion equations: Semi-analytical solutions

Abstract

Semi-analytical solutions for autocatalytic reactions with mixed quadratic and cubic terms are considered. The kinetic model is combined with diffusion and considered in a onedimensional reactor. The spatial structure of the reactant and autocatalyst concentrations are approximated by trial functions and averaging is used to obtain a lower-order ordinary differential equation model, as an approximation to the governing partial differential equations. This allows semi-analytical results to be obtained for the reaction–diffusion cell, using theoretical methods developed for ordinary differential equations. Singularity theory is used to investigate the static multiplicity of the system and obtain a parameter map, in which the different types of steady-state bifurcation diagrams occur. Hopf bifurcations are also found by a local stability analysis of the semi-analytical model. The transitions in the number and types of bifurcation diagrams and the changes to the parameter regions, in which Hopf bifurcations occur, as the relative importance of the cubic and quadratic terms vary, is explored in great detail. A key outcome of the study is that the static and dynamic stability of the mixed system exhibits more complexity than either the cubic or quadratic autocatalytic systems alone. In addition it is found that varying the diffusivity ratio, of the reactant and autocatalyst, causes dramatic changes to the dynamic stability. The semi-analytical results are show to be highly accurate, in comparison to numerical solutions of the governing partial differential equations.

Keywords

cubic, equations, mixed, quadratic, autocatalytic, reaction, diffusion, semi, analytical, solutions

Disciplines

Engineering | Science and Technology Studies

Publication Details

Alharthi, M., Marchant, T. R. and Nelson, M. I. (2014). Mixed quadratic-cubic autocatalytic reaction-diffusion equations: Semi-analytical solutions. Applied Mathematical Modelling, 38 (21-22), 5160-5173.

Mixed quadratic-cubic autocatalytic reaction-diffusion equations: semi-analytical solutions

M. R. Alharthi[1], T. R. Marchant*, M. I. Nelson

School of Mathematics and Applied Statistics, The University of Wollongong, Wollongong, 2522, N.S.W., Australia.

Abstract

Semi-analytical solutions for autocatalytic reactions with mixed quadratic and cubic terms are considered. The kinetic model is combined with diffusion and considered in a one-dimensional reactor. The spatial structure of the reactant and autocatalyst concentrations are approximated by trial functions and averaging is used to obtain a lower-order ordinary differential equation model, as an approximation to the governing partial differential equations. This allows semi-analytical results to be obtained for the reaction-diffusion cell, using theoretical methods developed for ordinary differential equations. Singularity theory is used to investigate the static multiplicity of the system and obtain a parameter map, in which the different types of steady-state bifurcation diagrams occur. Hopf bifurcations are also found by a local stability analysis of the semi-analytical model. The transitions in the number and types of bifurcation diagrams and the changes to the parameter regions, in which Hopf bifurcations occur, as the relative importance of the cubic and quadratic terms vary, is explored in great detail. A key outcome of the study is that the static and dynamic stability of the mixed system exhibits more complexity than either the cubic or quadratic autocatalytic systems alone. In addition it is found that varying the diffusivity ratio, of the reactant and autocatalyst, causes dramatic changes to the dynamic stability. The semi-analytical results are show to be highly accurate, in comparison to numerical solutions of the governing partial differential equations.

*Corresponding author

Email address: tim_marchant@uow.edu.au. (T. R. Marchant)

[1]This author is a PhD student at University of Wollongong (Assistant lecturer at University of Taif in Saudi Arabia)

Keywords: reaction-diffusion equations, autocatalytic reactions, singularity theory, Hopf bifurcations, semi-analytical solutions.

1. Introduction

Chemical reactions which display oscillatory solutions and multiple steady-state solutions have been of great interest to both theoreticians and experimentalists for over one hundred years. Some experimental examples of oscillatory behaviour in chemical systems include the Bray-Liebhafsky, Belousov-Zhabotinsky and Briggs-Rausher reactions, for which periodic variations in concentrations can be visualized via changes in colour; see [1] for a review of these reactions and other oscillatory phenomena. The most common reactor scenario in the literature, for the investigation of chemical systems, is the continuous flow well-stirred tank reactor (CSTR). Usually, a system of ordinary differential equations (odes) governs a CSTR, which can be analyzed by standard techniques. However the reaction-diffusion cell is also an important reactor scenario, which is governed by a system of partial differential equations (pdes), and not so easily analyzed.

A theoretical model with both quadratic and cubic autocatalysis with linear catalyst decay is considered in this work,

$$\begin{aligned} A + 2B &\to 3B, \quad \text{rate} = (1-\mathrm{p})\beta \mathrm{a}\mathrm{b}^2, \\ A + B &\to 2B, \quad \text{rate} = \mathrm{p}\beta \mathrm{a}\mathrm{b}, \\ B &\to C, \quad \text{rate} = \beta\gamma \mathrm{b}, \end{aligned} \tag{1}$$

where the concentrations of the reactant and autocatalyst are a and b, respectively. In (1) the first step is the cubic reaction, the second the quadratic reaction and the third represents linear decay of the catalyst. The reaction ratio $\mathrm{p} \in [0,\, 1]$ measures the strength of the quadratic reaction compared to the cubic reaction, where $p = 0$ is the cubic Gray-Scott model and $p = 1$ the quadratic limit. The mixed quadratic-cubic system is considered in this paper because its static and dynamic stability exhibits a wider variety of complex phenomena and structures that are much richer than either the cubic or quadratic schemes alone.

The mixed quadratic-cubic autocatalytic system (1) is a prototype system but [2] report that the iodate-arsenous acid reaction is an example of a mixed quadratic-cubic autocatalytic system where the cubic reaction dominates the quadratic limit. This system has been extensively studied due to appearance

of propagating wavefronts as the autocatalytically generated iodate spreads into regions with fresh reactant (arsenous acid). [2] found that instabilities develop when the ratio of reactant to autocatalyst diffusivities exceeds a critical value and found a good comparison between numerical solutions and experimental results. [3] modelled the iodate-arsenous acid reaction by the Dushman-Roebuck kinetic scheme and found appropriate conditions under which it could be modelled by a cubic autocatalytic rate law. The form of the travelling wave solution was shown to depend on the initial concentration ratio of reactant to autocatalyst.

[4] and [5] studied cubic autocatalysis ((1) when $p = 0$) in a CSTR. Three types of steady-state bifurcation diagrams occurred, the unique, mushroom and isola patterns, and they also identified the Hopf bifurcation parameter region. Numerical simulations of the ode model showed the evolution of the system to both stable and unstable limit-cycles and also the oscillatory decay to a stable steady state. [6] added an uncatalysed conversion step to (1) which increased the number of bifurcation diagrams to five. The two new bifurcation patterns were the breaking-wave and isola breaking-wave patterns, which both occurred in very small regions of parameter space. [7] and [8] studied the cubic autocatalytic system (1) in a reaction-diffusion cell. The pde model was solved numerically by discretization, which allowed four steady-state bifurcation diagrams to be identified. The breaking-wave isola pattern could not be found numerically, as its parameter region is too small. Moreover, they considered the stability of solutions, via the calculation of eigenvalues, for the discretized ode form of the governing pdes.

[9] found semi-analytical solutions for the Gray & Scott model in a reaction-diffusion cell. The Galerkin method was used to obtain a lower-order ode model, as an approximation to the governing pde system. Steady-state solutions and bifurcation diagrams were obtained for one-term and two-term approximations. Singularity theory was used to map the parameter space where the different bifurcation diagrams occurred. In addition, the region of parameter space where Hopf bifurcations occur was found by using a local stability analysis of the semi-analytical model. The semi-analytical results proved to be highly accurate and the method an effective alternative to the direct pde discretization used by [7]. [10] considered cubic autocatalysis in a 1-D reactor with the linear decay of the Gray & Scott model replaced by Michaelis–Menten catalyst decay, which is limited at high catalyst concentrations. The effect of varying the Michaelis constant, on the structure of the parameter maps describing Hopf bifurcations and bifurcation patterns

was explored. [11] considered the effect of the application of an electric field on the Gray & Scott model in a reaction-diffusion-advection cell. The electric field, modeled by advection terms in the governing equations, drives the migration of ions in the cell and changes the static and dynamic stability of the system. Its use as a possible feedback mechanism was investigated and it was found that it could act as a switch between high and low conversion states and changed the parameter map in which Hopf bifurcations occur.

The Galerkin method has also proved effective in solving reaction-diffusion problems with Arrhenius reaction terms, see [12] who developed semi-analytical solutions for 1-D and 2-D catalytic pellet problems. The semi-analytical model comprised a set of integro-differential equations which were used to obtain results for the static and dynamic stability of the pellet. The degenerate hysteresis and Hopf points were given by transcendental equations which included integrals, evaluated by numerical quadrature rules. The semi-analytical results were found be highly accurate when compared with exact, and computationally expensive, numerical bifurcation methods.

[13] showed that systems of two parallel or consecutive reactions, based on cubic or mixed quadratic and cubic autocatalysis, give rise to chaos. Lyapunov exponents were used to define ranges of parameter values for which chaotic behavior is possible. Chaos was found to occur over wide ranges of parameters values with very complicated transitions between chaos and periodicity occurring as the parameters are varied. A comparison was made between these autocatalytic systems and the analogous nonisothermal reaction systems for which chaotic behavior has previously been shown to be possible. [14] described the chaotic behavior produced by a reaction system composed of consecutive quadratic and cubic autocatalytic elementary steps. He showed that the existence of chaotic behavior does not depend on the presence of a reaction step involving cubic autocatalysis. [15] developed a linear stability analysis for a reactor model with a combination of quadratic and cubic steps and discussed the effect of adding an electrical field to the model. [16] gave a rigorous bifurcation analysis for a reactor model with both quadratic and cubic steps. They extended the analysis of [15] in two ways. Firstly, they imposed Dirichlet boundary conditions instead of considering the semi-infinite domain. Secondly, they considered a variety of different bifurcation phenomena of the corresponding steady state system, focusing on parametric sensitivity. They showed that the system exhibits subcritical and supercritical pitchfork bifurcations and transcritical bifurcation in the different regimes for the control parameters.

In this paper, a mixed quadratic-cubic autocatalytic scheme (1) is examined in a 1-D reaction-diffusion cell. Semi-analytical solutions are found using a Galerkin method, where a series of basis functions is used to model the spatial structure of the solution and hence reduce the pde system to an ode system. Whilst the cubic autocatalytic reaction-diffusion cell has been previously considered by [9] this paper investigates the changes to static and dynamic stability, for the mixed quadratic-cubic system, as the importance of the two types of reaction terms are varied. This study uncovers a great deal of additional complexity which is absent from either of the cubic or quadratic systems alone. In addition it is found that varying the diffusivity ratio, of the reactant and autocatalyst, has some dramatic effects on the dynamic stability.

In §2 the governing equations and boundary conditions are presented and described. The Galerkin method is applied to the governing equations to obtain the semi-analytical ode model. In §3 steady-state concentration profiles and bifurcation diagrams are shown and used to illustrate the complexity of the static multiplicity for this system and the accuracy of the semi-analytical solutions. In §4 singularity theory is applied to find the hysteresis and isola bifurcation points and map the regions of parameter space in which the five main bifurcation patterns occur. Varying the relative importance of the quadratic and cubic reactions results in changes in the number of bifurcation patterns while varying the diffusivity ratio of the two chemical species also changes the regions of parameter space. In §5 the stability of the semi-analytical model is considered. Both double-zero eigenvalue and transversally degenerate Hopf points are found and used to map the parameter regions in which Hopf bifurcations occur. Comparisons between the semi-analytical results and numerical solutions of the governing pdes are made, amnd illustrate the accuracy of the semi-analytical model. The appendix contains details of the ode models.

2. The semi-analytical model

2.1. The governing equations

The governing pdes for the mixed quadratic-cubic autocatalytic reaction with linear decay (1) in a 1-D reaction-diffusion cell are

$$a_t = \delta a_{xx} - p\beta ab - (1-p)\beta ab^2,\ b_t = b_{xx} + p\beta ab + (1-p)\beta ab^2 - \beta\gamma b,$$
$$a_x = b_x = 0 \text{ at x} = 0,\ \text{a} = 1,\ \text{b} = \text{b}_0 \text{ at x} = 1 \text{ and t} = 0, \qquad (2)$$

the concentrations of the reactant and autocatalyst given by a and b, respectively. The reactor boundary at $x = 1$ is permeable and connected to a reservoir of reactant and autocatalyst at constant concentrations. At $x = 0$ there is a zero-flux boundary condition. Alternatively a identical reservoir could be located at $x = -1$; the solution is then symmetric about the centre of the cell $x = 0$. The system is in non-dimensional form and has six parameters; b_0 is the autocatalyst reservoir concentration, $\beta(1-p)$ is the rate of the cubic reaction, βp the rate of the quadratic reaction, γ the rate of autocatalyst decay while δ is the diffusion coefficient for the reactant. The reaction ratio $p \in [0,1]$ measures the relative rates of the quadratic and cubic reactions. Choosing $p = 1$ will give a purely quadratic system while $p = 0$ gives the Gray & Scott cubic scheme. The parameters can be adjusted experimentally by changing the reservoir concentrations. Other possibilities for altering the parameters are discussed in [7], for example the diffusivity could be adjusted by adding inactive salts to the cell.

2.2. The Galerkin method

The Galerkin method uses a series of orthogonal basis functions to approximate the spatial structure of the concentration profiles. After the substitution of the basis functions the governing pdes (2) are then averaged to obtain a lower-order ode system. The expansion

$$\begin{aligned} a(x,t) &= 1 + a_1(t)\cos(\frac{1}{2}\pi x) + a_2(t)\cos(\frac{3}{2}\pi x), \\ b(x,t) &= b_0 + b_1(t)\cos(\frac{1}{2}\pi x) + b_2(t)\cos(\frac{3}{2}\pi x), \end{aligned} \tag{3}$$

represents the two-term method. It was found in [9] that a one-term solution (when $a_2 = b_2 = 0$) is not sufficiently accurate and that a two-term method is needed. (3) satisfies the boundary conditions in (2). The governing pdes are not satisfied exactly but in an averaged sense. The free parameters in (3) are found by evaluating averaged versions of the governing equations, weighted by the basis functions. This gives the odes

$$\begin{aligned} &\frac{d}{dt}a_1 = -N_1\beta - \frac{1}{4}\delta a_1\pi^2, \frac{d}{dt}b_1 = N_1\beta - \frac{1}{4}b_1\pi^2 - \beta\gamma(\frac{4b_0}{\pi} + b_1), \\ &\frac{d}{dt}a_2 = -N_2\beta - \frac{9}{4}\delta a_2\pi^2, \frac{d}{dt}b_2 = N_2\beta - \frac{9}{4}b_2\pi^2 - \beta\gamma(b_2 - \frac{4b_0}{3\pi}), \end{aligned} \tag{4}$$

where N_1 and N_2 are given in Appendix A.

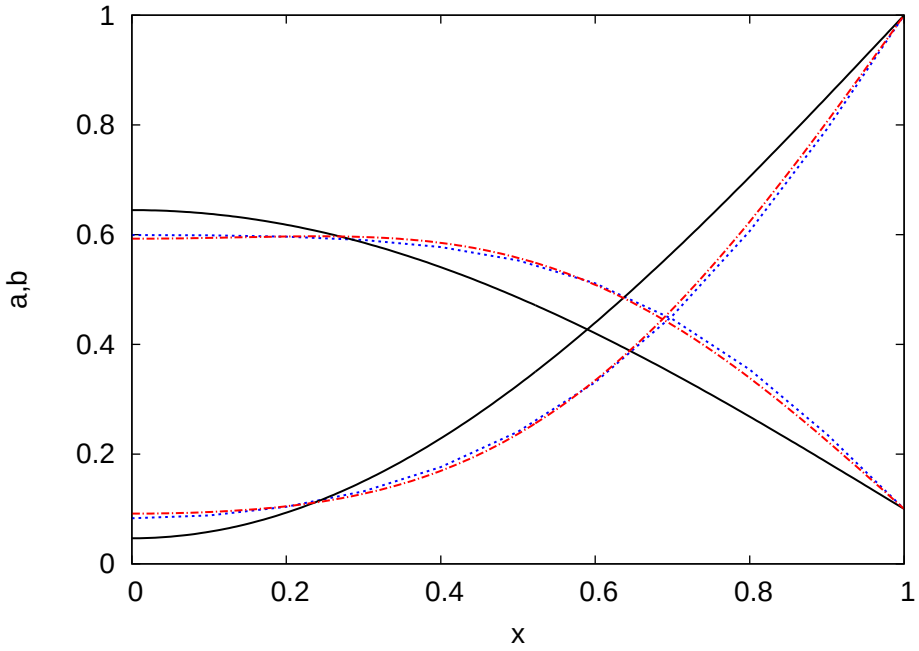

Figure 1: (Color online) Steady-state reactant and autocatalyst concentration profiles, a and b versus x. The parameters are $b_0 = 0.1$, $\gamma = 0.05$, $\beta = 40$, $\delta = 1$ and $p = 0.2$. The one-term (black solid line) and two-term (red large dashes) semi-analytical solutions and the numerical solution of (2) (blue small dashes) are shown.

3. Steady-state solutions

In this section we consider the steady-state versions of (4), where $\frac{da_1}{dt} = \frac{da_2}{dt} = \frac{db_1}{dt} = \frac{db_2}{dt} = 0$. This is a set of four transcendental equations, which are solved numerically using Maple. For the one term case, $a_2 = b_2 = 0$. Figure 1 shows steady-state concentration profiles of the reactant and the autocatalyst, a and b versus x. The parameters are $b_0 = 0.1$, $\gamma = 0.05$, $\beta = 40$, $\delta = 1$ and $p = 0.2$. The one-term, two-term semi-analytical and numerical solutions of (2) are shown. It can be seen that the two-term expression gives a good approximation when compared with the numerical solution of the governing pdes. At the center of the cell, the errors are only 0.66% and 0.85% for the autocatalyst and reactant concentrations respectively. For the one-term approximation, the errors are 3.6% and 4.5% for the autocatalyst and reactant concentrations. As reactant is consumed and autocatalyst created

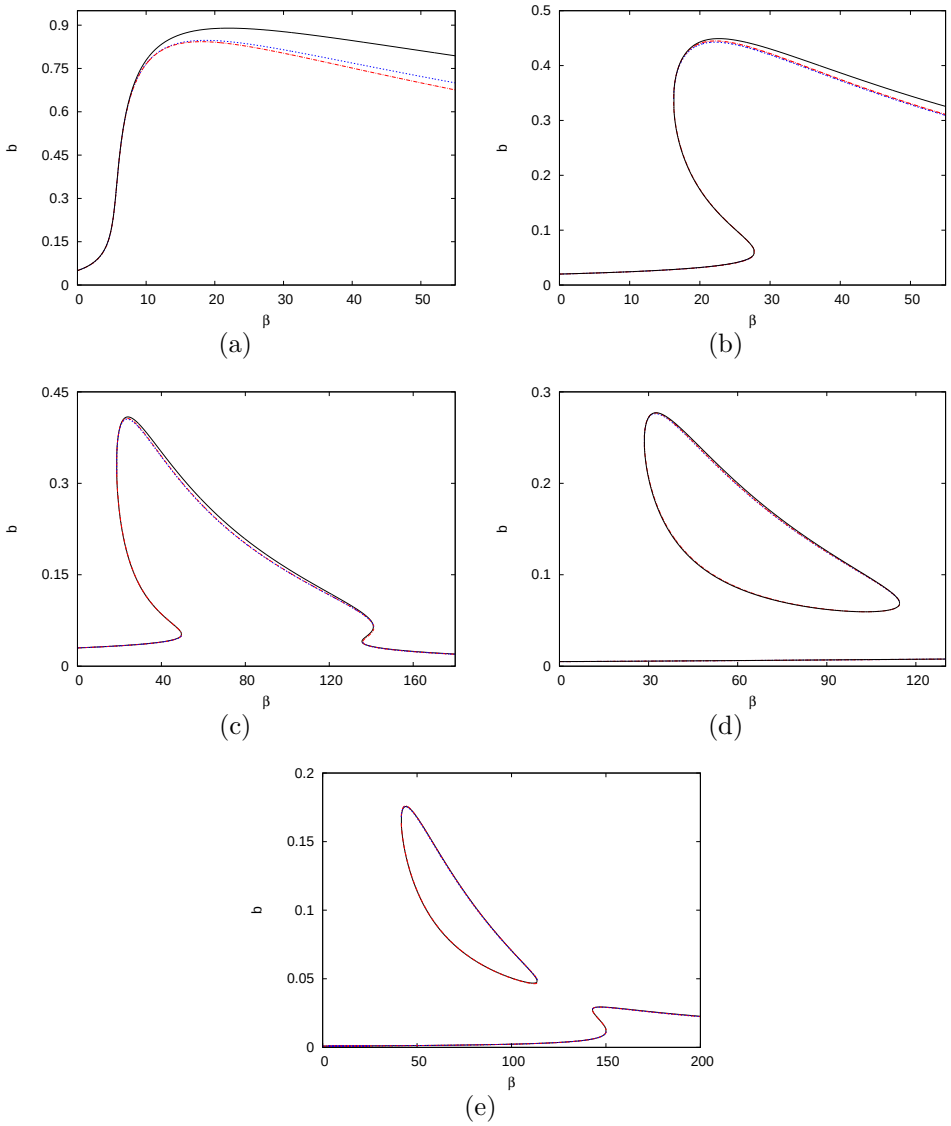

Figure 2: (Color online) Steady-state bifurcation diagrams; the autocatalyst concentration, b versus β when $\delta = 1$, (a) the unique pattern, with $b_0 = 0.05, \gamma = 0.018$ and $p = 0.3$; (b) the breaking-wave pattern with $b_0 = 0.02, \gamma = 0.065$ and $p = 0.08$; (c) the mushroom pattern, with $b_0 = 0.03, \gamma = 0.069$ and $p = 0.05$; (d) the isola pattern, with $b_0 = 0.005, \gamma = 0.078$ and $p = 0.08$ and (e) the isola breaking wave pattern, with $b_0 = 0.0009, \gamma = 0.0873$ and $p = 0.1$. The one-term (black solid lines) and two-term (red large dashes) semi-analytical solutions plus the numerical solution of (2) (blue small dashes) are shown.

by the reaction, the concentrations of reactant is lower and autocatalyst higher, than the boundary values, in the center of the cell.
Figure 2 shows steady-state bifurcation diagrams representing the five generic patterns. They are the (a) unique pattern, (b) breaking-wave pattern, (c) mushroom pattern,(d) isola pattern, and (e) isola breaking wave pattern. The bifurcation diagrams show the steady-state autocatalyst concentration at the reactor's center, b, versus the bifurcation parameter β. The one-term and two-term semi-analytical solutions plus the numerical solution of (2) are shown. It can be seen that the two-term solution is very close to the numerical solution of the pdes. For the purely cubic case numerical and analytical studies show that, the isola breaking wave bifurcation pattern occurs in an extremely small parameter region of parameter space, see [7] and [9]. For the mixed quadratic-cubic model, the five generic types of bifurcation diagrams are easily found, as increasing the ratio p makes the isola breaking wave pattern more easily discoverable.

4. Singularity theory

Singularity theory can be used to determine the regions of parameter space in which qualitatively distinct bifurcation patterns occur, for a system of odes. [17] applied singularity theory to a system of two coupled odes with three independent parameters by plotting the locus of successively degenerate points in order to build up a full description of the system. [18] applied the methodology of singularity theory to CSTR systems and gave conditions for the calculation of the hysteresis and isola bifurcation curves. Here singularity theory will be used to analyze the semi-analytical model of §2, which consists of odes. Hence a semi-analytical map of the parameter regions in which the different bifurcation patterns occur, is found. At the steady-state the two-term model has the general form

$$f_i(b_0, b_1, b_2, a_1, a_2, p, \delta, \beta, \gamma) = 0, \quad i = 1 \ldots 4, \tag{5}$$

where β is the bifurcation parameter. Note that here the parameters a_1, a_2, b_1, b_2 are the steady-state solutions of the system of odes (4). Solutions for which a hysteresis loop or fold first occurs in the bifurcation diagram correspond to hysteresis bifurcation points. These are given by the conditions

$$\frac{d\beta}{db_1} = \frac{d^2\beta}{db_1^2} = 0, \tag{6}$$

The conditions (6) must be applied by using implicit differentiation as an explicit expression for β is not available. This is done by taking the total derivative of (5) with respect to b_1 whilst holding the parameters γ, p, δ and b_0 constant and also applying while the first of (6), $\frac{d\beta}{db_1} = 0$. This gives

$$\frac{df_i}{db_1}(b_1, b_2, a_1, a_2) = f_{i_{b1}} + f_{i_{b2}}\frac{db_2}{db_1} + f_{i_{a1}}\frac{da_1}{db_1} + f_{i_{a2}}\frac{da_2}{db_1} = 0, \quad i = 1 \ldots 4, \quad (7)$$

In a similar manner the second total derivative of (5) and conditions (6) give

$$\frac{d^2 f_i}{db_1^2}(b_1, b_2, a_1, a_2) = 0, \quad i = 1 \ldots 4, \quad (8)$$

The two-term hysteresis bifurcation points are given by (5), (7) and(8), which from a set of twelve equations for the fifteen variables b_1, b_2, a_1, a_2, β, γ, b_0, $\frac{db_2}{db_1}$, $\frac{d^2b_2}{db_1^2}$, $\frac{da_1}{db_1}$, $\frac{d^2a_1}{db_1^2}$, $\frac{da_2}{db_1}$, $\frac{d^2a_2}{db_1^2}$, p and δ . The implicit differentiation has introduced six new variables. We take fixed values of p and δ and consider the loci of points, which form a line in the γ-b_0 plane. If this line is crossed then a hysteresis loop is created or destroyed in the relevant bifurcation diagram. The sets of transcendental equations for the hysteresis bifurcation points are solved using Maple. A similar methodology is used to obtain the relevant sets of transcendental equations for the isola bifurcation curve, the isola hysteresis point and the double-zero eigenvalue (DZE) and transversality Hopf degenerate curves. The isola bifurcation points are given by

$$\frac{d\beta}{db_1} = \frac{d\gamma}{d\beta} = 0, \quad (9)$$

If the isola bifurcation curve, a line in the γ-b_0 plane, is crossed then an isola is created or destroyed in the bifurcation diagram. Varying the parameters $p \in [0, 1]$ and $\delta \in [0, \infty)$ results in significant changes to the parameter regions in which the various types of bifurcation patterns occur.

4.1. The effect of varying the reaction ratio p

In this subsection we consider the effect of varying the ratio p, which describes the relative importance of the quadratic and cubic reactions. The semi-analytical model can be used to quantify the transitions in the number of bifurcation patterns, and changes to parameter regions, as p varies. Table 1 shows the values of p for which the different types of steady-state solutions

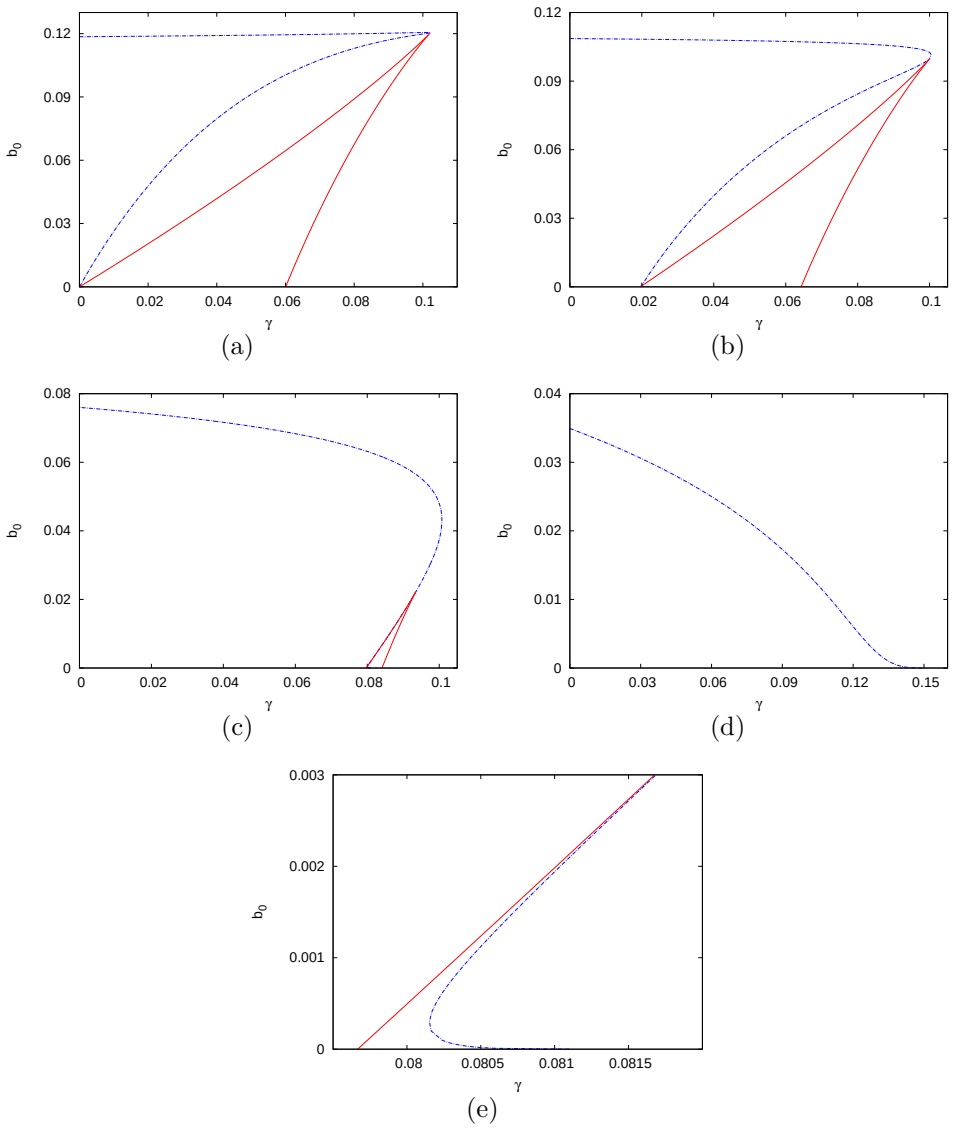

Figure 3: (Color online) Division of the γ-b_0 plane into regions corresponding to the different bifurcation diagrams,(a) $p = 0$, (b) $p = 0.02$, (c) $p = 0.09$, (d) $p = 0.2$ and (e) the small region in (c) $p = 0.09$. The isola curves (red solid lines) and the hysteresis curves (blue small dashes) are shown

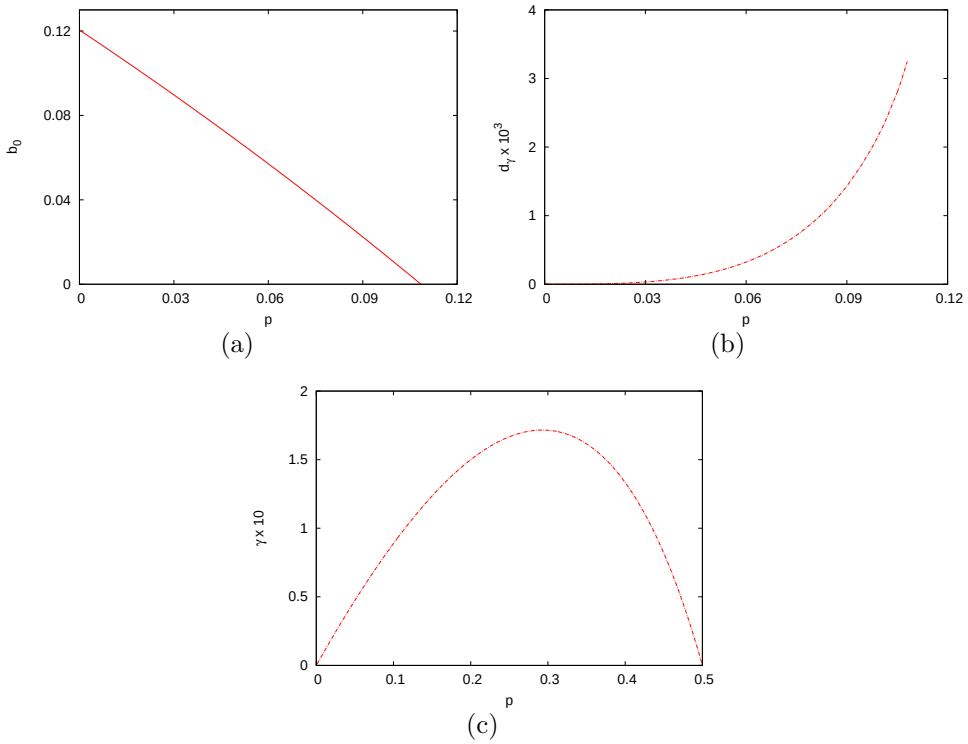

Figure 4: Transitions in the γ-b_0 plane as p varies. (a) The maximum point of the isola curve b_0 verses p, (b) the absolute distance between the hysteresis and the isola curve when $b_0 = 0$, d_γ versus p, and (c) the intersection point of the hysteresis curve with $\gamma-$axis when $b_0 = 0$.

p	Number	Type
$0 \leq p \lesssim 0.0806$	5	a,b,c,d,e
$0.0806 \lesssim p \lesssim 0.108$	4	a,b,d,e
$0.1084 \lesssim p \lesssim 0.5$	2	a,b
$0.5 \lesssim p \leq 1$	1	a

Table 1: Numbers and types of steady-state bifurcation diagrams when $p \in [0, 1]$

occur. It can be clearly seen that there are richer behaviors for small p, when cubic terms dominate and less complexity as p increases when quadratic reaction term dominate. In table 1 the types of behaviors are labeled the (a) unique pattern, (b) breaking-wave pattern, (c) mushroom pattern,(d) isola pattern, and (e) isola breaking wave pattern.
Figure 3 shows the division of the γ-b_0 plane into regions corresponding to the different bifurcation diagrams when (a) $p = 0$, (b) $p = 0.02$, (c) $p = 0.09$ and (d) $p = 0.2$. In (e), the small region in (c) is shown where the isola breaking wave pattern appears. We can clearly see that as the reaction ratio p changes that dramatic changes in the regions occur. For the purely cubic case when $p = 0$, [9] mentioned that there are four kinds of steady-state bifurcation diagrams.They are the unique, breaking-wave, mushroom and the isola pattern. He also found that, in the semi-analytical model, a fifth bifurcation diagram occurs in an extremely small parameter region; its size being $O(10^{-10})$. As p increases from zero, the parameter region in which the fifth pattern occur grows and the region in which the mushroom pattern occurs, becomes narrower. The isola and hysteresis curves move downwards, as p increases. When $p \approx 0.0806$, the mushroom pattern disappears and at $p \approx 0.108$, the isola curve moves completely to the negative region of the γ-b_0 plane (negative values of the parameters are unphysical). For p>0.108 the hysteresis curve divides the γ-b_0 plane into two regions where, the unique and the breaking-wave pattern occur. Finally, when $p = 0.5$, the hysteresis curve also moves into the negative b_0-plane and for p>0.5, only one type of steady state bifurcation diagram occurs, which is the unique pattern.

Figure (4) illustrates some of the important singularity theory transitions in the γ-b_0 plane, that occur as p varies. Figure 4(a) shows the maximum point of the isola curve b_0 versus p. At $p = 0$ the maximum point is $b_0 \approx 0.12$ (see figure 3(a)). As p increases, this maximum decreases until $p \approx 0.108$ when it moves to the negative b_0-plane. Figure 4(b) shows the distance, d_γ, between the hysteresis curve and the isola curve at $b_0 = 0$, d_γ versus p. d_γ is a measure of the size of the parameter region in which the fifth bifurcation pattern appears as shown in figure 3(e), where $d_\gamma \approx 0.0014$ at $p = 0.09$. This difference at $p = 0$ is $d_\gamma = 0$ and it grows to $d_\gamma \approx 0.0033$ when $p \approx 0.108$, where the isola curve disappears from the positive b_0-plane.

Figure 4(c) shows the intersection point of the hysteresis curve with γ - axis. This intersection point starts at$\gamma = 0$ when $p = 0$ (see figure 3(a)) and moves to a maximum of $\gamma \approx 0.171$ when $p \approx 0.293$, before retreating back

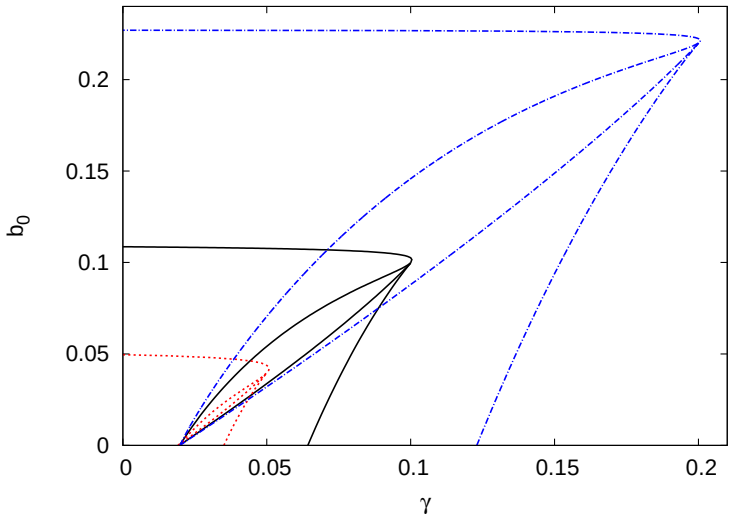

Figure 5: (Color online) The division of the γ-b_0 plane into regions corresponding to the different bifurcation diagrams when $p = 0.02$ and $\delta = 0.5$(red small dashes), $\delta = 1$(black solid line) and when $\delta = 2$ (blue large dashes)

to $\gamma = 0$ at $p = 0.5$, when the hysteresis curve disappears from the positive γ-b_0 plane.

4.2. The effect of varying the diffusivity ratio δ

Varying the diffusivity ratio δ effects the regions of parameter space in which the bifurcation patterns occur. Figure 5 shows the division of the γ-b_0 plane into regions corresponding to the different bifurcation diagrams for different values of δ, when $p = 0.02$. When δ increases, the hysteresis and isola curves expand but maintain a similar shape. For the pure cubic reaction, $p = 0$, the isola and hysteresis curves are self similar for all values of δ>0, so for small p, they have qualitatively similar shapes. For $\delta < 1$ the curve shrinks. Hence the smaller the diffusivity of the reactant a, the smaller the parameter region in which multiple steady-state solutions can occur.

5. Local stability and oscillatory solutions

The local stability of ode systems can be found by calculating the eigenvalues of the Jacobian matrix, which govern the growth of small perturba-

tions. Bifurcation theory, dynamical systems and limit cycles are discussed in many texts, for example see [19] or [20]. For the cubic autocatalytic system ((1) when $p = 0$), both the CSTR and the reaction-diffusion cell exhibit Hopf bifurcations, see [4] and [9]. Here the stability of the semi-analytical model of the mixed quadratic-cubic system is considered by finding the Hopf degenerate points and mapping these in parameter space.

For the one-term case the semi-analytical model (4) reduces to pair of odes for a_1 and b_1. In this case the eigenvalues of the Jacobian matrix are governed by a quadratic equation

$$\lambda^2 + \alpha_1\lambda^2 + \alpha_2 = 0, \tag{10}$$

with the degenerate Hopf points given by

$$DZE : f_i = \alpha_1 = \alpha_2 = 0, H2 : f = \alpha_1 = \frac{d\alpha_1}{d\beta} = 0, i = 1, 2 \tag{11}$$

The two-term semi-analytical model is a set of four odes (4), with the eigenvalues of the Jacobian matrix given by the quartic equation,

$$\lambda^4 + \alpha_1\lambda^3 + \alpha_2\lambda^2 + \alpha_3\lambda + \alpha_4 = 0, \tag{12}$$

If it is assumed that one pair of eigenvalues in (12) are purely imaginary then Hopf bifurcations occur. The degenerate Hopf points are given by

$$DZE : f_i = \alpha_3 = \alpha_4 = 0, H2 : f_i = q = \frac{dq}{d\beta} = 0, i = 1, 4 \tag{13}$$
$$\text{where } \; q = \alpha_4\alpha_1^2 + \alpha_3^2 - \alpha_1\alpha_2\alpha_3 = 0.$$

By solving the DZE and H2 conditions, we obtain curves in the $\gamma - b_0$ plane. We will discuss the effect of varying the reaction ratio p and the diffusivity ratio δ on the occurrence of Hopf bifurcations.

Figure 6 shows the Hopf bifurcation curves in the γ-b_0 plane, for $p = 0$, $p = 0.05$ and $p = 0.1$ when $\delta = 1$. The maximum height of the Hopf bifurcation curves are $b_0 \approx 0.148, 0.079, 0.029$ for $p = 0, 0.05, 0.1$ respectively. The area confined by the Hopf curve shrinks, as p increases and it moves completely into the negative b_0 plane at $p \approx 0.19$. Hence for $p \gtrsim 0.19$, Hopf bifurcations do not occur and no oscillatory solutions are possible.

Figure 7 shows Hopf curves for various values of δ. Figure 7(a) shows $\delta = 1, 2$ and 3, 7(b) $\delta = 0.75$ and 7(c) $\delta = 0.5$. For $\delta \geq 1$, there is only

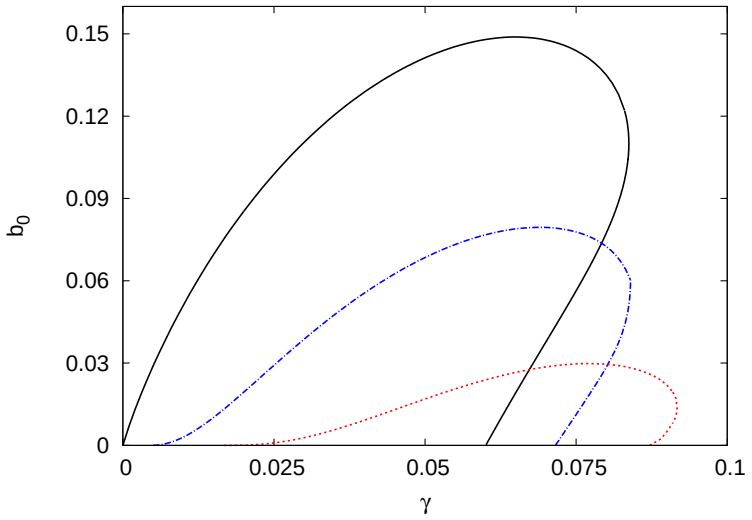

Figure 6: Hopf curve when $p = 0$ (black solid line), $p = 0.05$ (blue large dashes) and $p = 0.1$ (red small dashes)

one Hopf curve and it expands in area as δ increases. Hence large diffusivity of the reactant a leads to an increased possibility of Hopf bifurcations and oscillatory solutions. For $\delta < 1$, the picture is more complex as a second Hopf curve appears in the $\gamma - b_0$ plane, which increases in area as δ decreases.

Figure 8 shows the H2 and DZE curves which divide the γ-b_0 plane into regions corresponding to the number of Hopf points that the steady-state diagrams have, when $\delta = 0.25$. In this figure, there are two regions which have four Hopf points in the steady-state diagram, one region has three Hopf points, three regions have two Hopf points, two regions have only one Hopf points and one region for which the steady-state diagram has no Hopf points. Moving across H2 curves results in the appearance or disappearance of two Hopf points, while moving across the DZE curves results in the appearance or disappearance of one Hopf point. There are two intersection points between the H2 curves as shown in figure 8. They are $(\gamma, b_0) \approx (0.0101, 0.0435)$, which gives a unique steady-state pattern, and $(0.00902, 0.0093)$, which gives an isola steady-state pattern. The values of the bifurcation parameter for these points are $\beta = 26, 1204$ and $\beta = 154, 267$ respectively.

Figure 9(a) shows a limit cycle curve, a versus b, while 9(b) and 9(c)

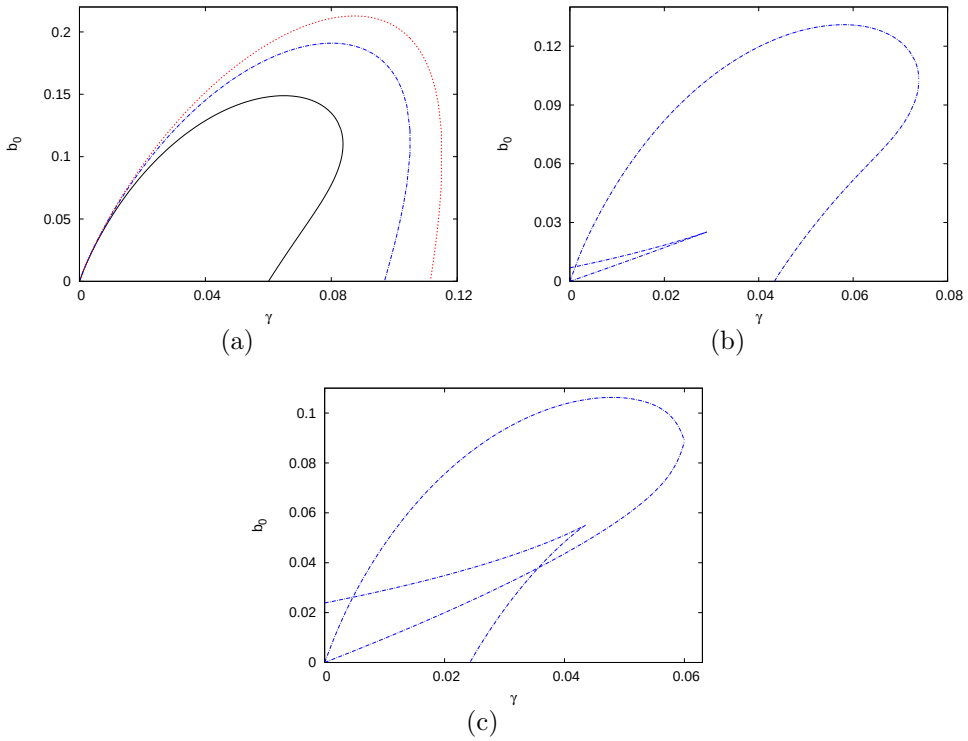

Figure 7: (Color online) Hopf curves for different values of δ,(a) when $\delta = 1, 2, 3$, (b) when $\delta = 0.75$ and (c) when $\delta = 0.5$.

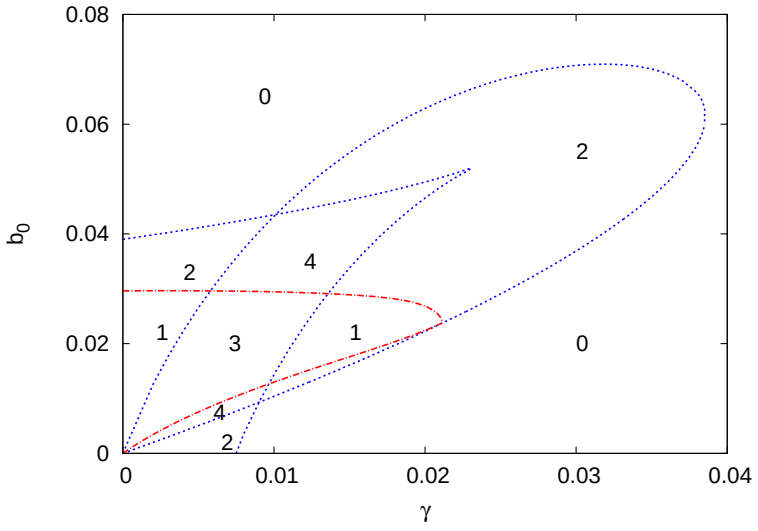

Figure 8: (Color online) Division of the γ-b_0 plane into regions corresponding to the number of Hopf points that steady-state diagrams have, where H2 curve (small dashes) and DZE curve (large dashes)when $\delta = 0.25$ and $p = 0$.

show the time evolution of the reactant and autocatalyst, a and b versus t respectively. The parameters are $b_0 = 0.02$, $\gamma = 0.07$, $\beta = 300$, $\delta = 1$ and $p = 0.1$. This limit cycle occurs in a portion of parameter space for which a limit cycle does not occur in the case of a purely cubic reaction ($p = 0$). The one term, two-term semi-analytical solutions and the numerical solutions of (2) are shown. The numerical period of the limit cycle is 0.901 while, the amplitudes of the limit cycle are 0.417 and 0.111 for the reactant and autocatalyst concentrations respectively. The two-term semi-analytical period and amplitude are very close to the numerical results, where the period is 0.997 and the amplitudes are 0.399 and 0.1035 for the reactant and autocatalyst concentrations respectively. The errors in the two-term semi-analytical values are less than 2%.

Figure 10(a) shows a limit cycle curve a versus b, while 10(b) and 10(c) show the time evolution of reactant and autocatalyst, a and b versus t respectively. The parameters are $b_0 = 0.035$, $\gamma = 0.003$, $\beta = 26$, $p = 0$ and $\delta = 0.25$. The one term, two-term semi-analytical solutions and the numerical solutions of (2) are shown. This limit cycle occurs in a section of parameter space, for

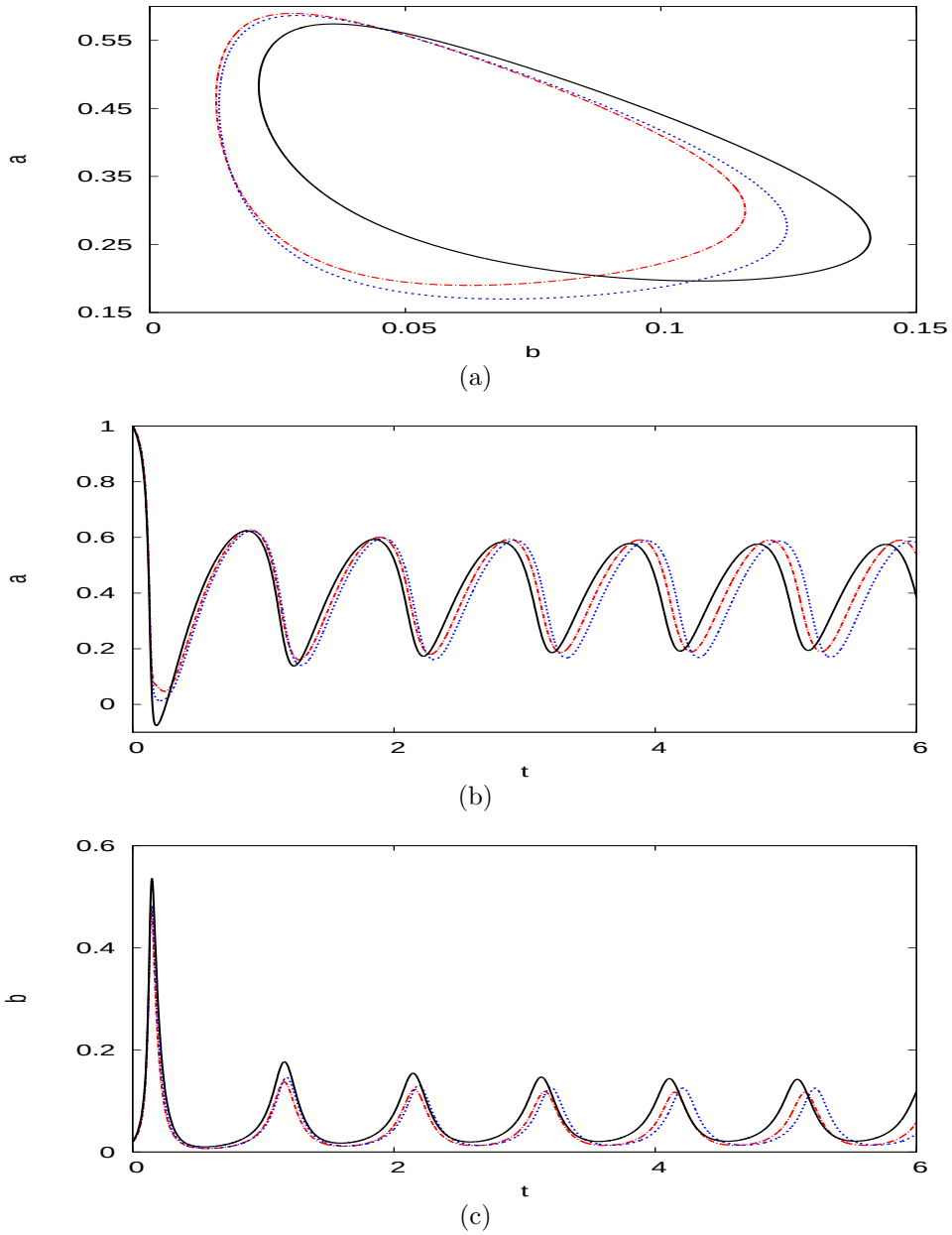

Figure 9: (Color online) (a) The limit cycle curve a versus b, (b) and (c) the reactant and autocatalyst concentration profiles, a and b at $x = 0$ versus t respectively. The parameters are $b_0 = 0.02$, $\gamma = 0.07$, $\beta = 300$, $\delta = 1$ and $p = 0.1$. The one-term (black solid line), the two-term (red large dashes) semi-analytical solutions and the numerical solution of (2) (blue small dashes) are shown.

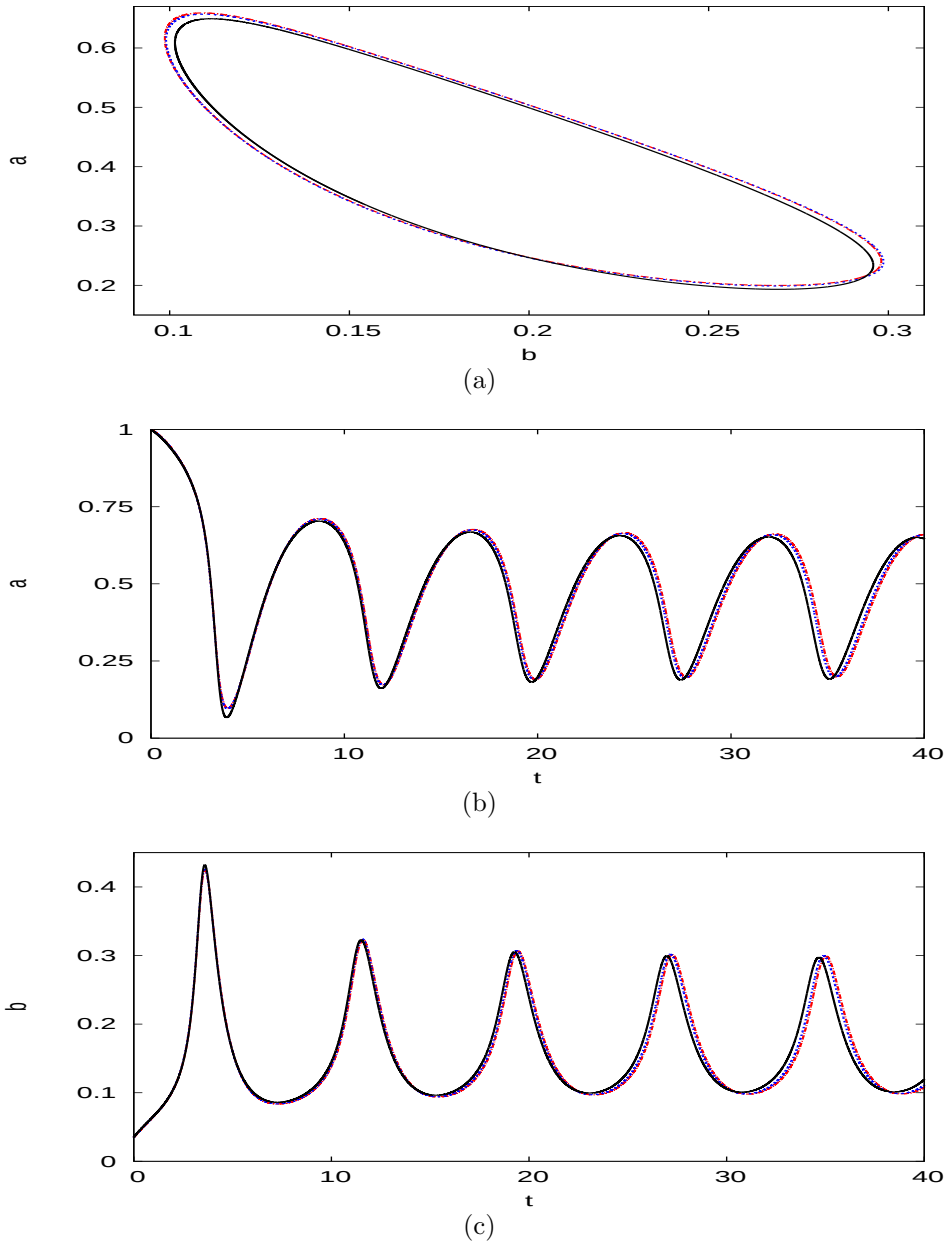

Figure 10: (Color online) (a) The limit cycle curve a versus b, (b) and (c) the reactant and autocatalyst concentrations, a and b at $x = 0$ versus t respectively. The parameters are $b_0 = 0.035$, $\gamma = 0.003$, $\beta = 26$, $p = 0$ and $\delta = 0.25$. The one-term (black solid line), the two-term (red large dashes) semi-analytical solutions and the numerical solution of (2) (blue small dashes) are shown.

which Hopf bifurcations do not occur when $\delta = 1$. Hence, the reduction of the diffusivity ratio δ has resulted in this new region of parameter space being subject to Hopf bifurcation. The numerical period of the limit cycle is 7.74 while, the amplitudes of the limit cycle are 0.458 and 0.1996 for the reactant and autocatalyst concentrations respectively. The two-term semi-analytical period and amplitude are very close to the numerical results; the period is 7.77 and the amplitudes are 0.459 and 0.1993 for the reactant and autocatalyst concentrations respectively. The errors in the two-term semi-analytical values are less than 0.4%.

Figure 11 shows the reactant and autocatalyst concentrations, a and b at $x = 0$ versus t in 11(a) and 11(b) respectively. The parameters are $b_0 = 0.02$, $\gamma = 0.06$, $\beta = 50$, $p = 0.15$ and $\delta = 0.25$. The one term, two-term semi-analytical solutions and the numerical solutions of (2) are shown. The solutions evolve to the steady-states for large time, with $a(0,t) = 0.36008$ and $b(0,t) = 0.07639$. Some initial relaxation oscillations occur for small time. It can be seen that the two-term expression gives a good approximation when compared with the numerical solution of the governing pdes. At $t = 12$, the one-term errors are 1.25% and 0.4% for the reactant and autocatalyst concentrations respectively, while for two-term semi-analytical approximations, the errors are 0.3% and 0.05% for the reactant and autocatalyst concentrations respectively.

6. Conclusion

The reaction-diffusion cell scenario has been used in this paper to explore the mixed quadratic-cubic autocatalytic reaction. The effect of varying the diffusivity of the two chemical species and the relative rates of the quadratic and cubic reactions have been considered in great detail. The mixed model is shown to exhibit a wide variety of complexity, both for bifurcation patterns and Hopf points. This study maps and quantifies the transitions that occur between the pure cubic and pure quadratic systems. Varying the diffusivity of the reactant uncovers new features in the parameter map for Hopf bifurcations, that do not occur for the equal diffusivity case. The averaging method used here has proved highly effective in analyzing the reaction-diffusion cell. A number of extensions are possible in further work such as circular or rectangular cell geometries. Feedback control, via the alteration of the reservoir concentrations, in response to the concentration in the cell, would also be of

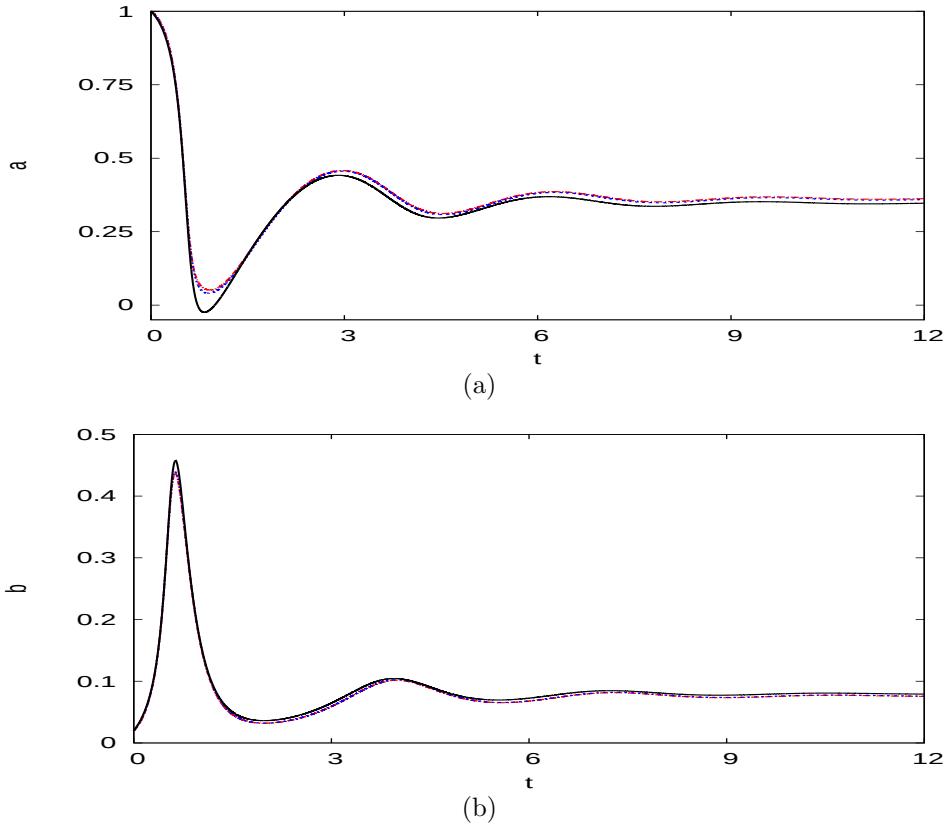

Figure 11: (Color online) The reactant and autocatalyst concentrations, a and b at $x = 0$ versus t in (a) and (b) respectively. The parameters are $b_0 = 0.02$, $\gamma = 0.06$, $\beta = 50$, $p = 0.15$ and $\delta = 0.25$. The one-term (black solid line), the two-term (red large dashes) semi-analytical solutions and the numerical solution of (2) (blue small dashes) are shown.

great interest for this system as it would allow the dynamic stability to be modified or controlled.

Appendix A. The ode model

Details of the expressions N_1, and N_2, in (4) are given

$$
\begin{aligned}
N_1 &= \frac{-1}{2} p a_1 {b_2}^2 - \frac{72}{35}\frac{p{b_2}^2}{\pi} - p a_2 b_1 b_2 + p a_1 b_0 + 4\frac{p b_0}{\pi} + \frac{16}{15}\frac{a_1 b_0 b_2}{\pi} \\
&+ \frac{16}{15}\frac{a_2 b_0 b_1}{\pi} + \frac{16}{3}\frac{a_1 b_0 b_1}{\pi} - \frac{16}{15}\frac{p b_1 b_2}{\pi} + \frac{144}{35}\frac{a_2 b_0 b_2}{\pi} - \frac{1}{2} p a_1 b_1 b_2 \\
&- 2\, p b_0 b_1 - \frac{3}{4} p a_1 {b_1}^2 - \frac{8}{3}\frac{p{b_1}^2}{\pi} - \frac{1}{4} p a_2 {b_1}^2 + p b_1 + a_2 b_1 b_2 \\
&+ \frac{16}{15}\frac{b_1 b_2}{\pi} + \frac{1}{2} a_1 b_1 b_2 - p a_1 {b_0}^2 - 4\frac{p{b_0}^2}{\pi} - \frac{144}{35}\frac{p a_2 b_0 b_2}{\pi} + \frac{72}{35}\frac{p a_2 b_2}{\pi} \\
&+ \frac{8}{15}\frac{p a_1 b_2}{\pi} + \frac{8}{15}\frac{p a_2 b_1}{\pi} + \frac{8}{3}\frac{p a_1 b_1}{\pi} - \frac{16}{3}\frac{p a_1 b_0 b_1}{\pi} - \frac{16}{15}\frac{p a_1 b_0 b_2}{\pi} \\
&- \frac{16}{15}\frac{p a_2 b_0 b_1}{\pi} + 4\frac{{b_0}^2}{\pi} + a_1 {b_0}^2 + \frac{3}{4} a_1 {b_1}^2 + \frac{8}{3}\frac{{b_1}^2}{\pi} + \frac{72}{35}\frac{{b_2}^2}{\pi} \\
&+ \frac{1}{2} a_1 {b_2}^2 + 2\, b_0 b_1 + \frac{1}{4} a_2 {b_1}^2, \qquad \text{(A.1)} \\
N_2 &= -2\, p b_0 b_2 + \frac{8}{9}\frac{p{b_2}^2}{\pi} - \frac{4}{3}\frac{p b_0}{\pi} + \frac{144}{35}\frac{a_1 b_0 b_2}{\pi} + \frac{144}{35}\frac{a_2 b_0 b_1}{\pi} \\
&+ \frac{16}{15}\frac{a_1 b_0 b_1}{\pi} - \frac{144}{35}\frac{p b_1 b_2}{\pi} - \frac{16}{9}\frac{a_2 b_0 b_2}{\pi} - p a_1 b_1 b_2 + p a_2 b_0 - \frac{1}{4} p a_1 {b_1}^2 \\
&- \frac{8}{15}\frac{p{b_1}^2}{\pi} - \frac{1}{2} p a_2 {b_1}^2 + \frac{144}{35}\frac{b_1 b_2}{\pi} + a_1 b_1 b_2 - \frac{3}{4} p a_2 {b_2}^2 + \frac{4}{3}\frac{p{b_0}^2}{\pi} \\
&- p a_2 {b_0}^2 + p b_2 + \frac{16}{9}\frac{p a_2 b_0 b_2}{\pi} - \frac{8}{9}\frac{p a_2 b_2}{\pi} + \frac{72}{35}\frac{p a_1 b_2}{\pi} + \frac{72}{35}\frac{p a_2 b_1}{\pi} \\
&+ \frac{8}{15}\frac{p a_1 b_1}{\pi} - \frac{16}{15}\frac{p a_1 b_0 b_1}{\pi} - \frac{144}{35}\frac{p a_1 b_0 b_2}{\pi} - \frac{144}{35}\frac{p a_2 b_0 b_1}{\pi} - \frac{4}{3}\frac{{b_0}^2}{\pi} \\
&+ \frac{1}{4} a_1 {b_1}^2 + \frac{8}{15}\frac{{b_1}^2}{\pi} - \frac{8}{9}\frac{{b_2}^2}{\pi} + \frac{1}{2} a_2 {b_1}^2 + a_2 {b_0}^2 + \frac{3}{4} a_2 {b_2}^2 + 2\, b_0 b_2
\end{aligned}
$$

Acknowledgements

M. Alharthi gratefully thanks Taif university in Saudi Arabia for awarding him a PhD scholarship to study at the University of Wollongong, Australia.

References

[1] J. M. L. Corbel, J. N. J. Van Lingen, J. F. Zevenbergen, O. L. J. Gijzeman, A. Meijerink, Strobes: pyrotechnic compositions that show a curious oscillatory combustion, Angew. Chem. Int. Ed. 52 (2013) 290–303.

[2] D. Horvath, K. Showalter, Instabilities in propagating reaction-diffusion fronts of the iodate-arsenous acid reaction, J. Chem. Phys. 102 (1995) 2471–2478.

[3] J. H. Merkin, H. Sevcikova, Travelling waves in the iodate-arsenous acid system, Phys. Chem. Chem. Phys. 1 (1999) 91–97.

[4] P. Gray, S. K. Scott, Autocatalytic reactions in the isothermal continuous, stirredtank reactor: isolas and other forms of multistability, Chem. Engng. Sci. 38 (1983) 29–43.

[5] P. Gray, S. K. Scott, Autocatalytic reactions in the isothermal continuous, stirredtank reactor: oscillations and instabilities in the system $a + 2b \rightarrow 3b; b \rightarrow c$, Chem. Engng. Sci. 39 (1984) 1087–1097.

[6] S. R. Kay, S. K. Scott, P. G. Lignola, The application of singularity theory to isothermal autocatalyticreactions: the influence of uncatalysed reactions, Proc. Roy. Soc. Lond A 409 (1987) 433–448.

[7] S. K. Scott, Isolas, mushrooms and oscillations in isothermal, autocatalyticreaction-diffusion equations, Chem. Engng. Sci. 42 (1987) 307–315.

[8] S. R. Kay, S. K. Scott, Multiple stationary states, sustained oscillations and transientbehavior in autocatalytic reaction-diffusion equations, Proc. Roy. Soc. Lond A 418 (1988) 345–364.

[9] T. R. Marchant, Cubic autocatalytic reaction-diffusion equations:semi-analytical solutions, Proc. Roy. Soc. Lond A 458 (2002) 873–888.

[10] T. R. Marchant, Cubic autocatalysis with Michaelis-Menten kinetics: semi-analytical solutions for the reaction-diffusion cell, Chem. Engng. Sci. 59 (2004) 3433–3440.

[11] A. Thornton, T. Marchant, Semi-analytical solutions for a Gray-Scott reaction-diffusion cell with an applied electric field, Chem. Engng. Sci. 63 (2008) 495–502.

[12] T. R. Marchant, M. I. Nelson, Semi-anlaytical solutions for one and two-dimensional pellet problems, Proc. Roy. Soc. Lond A 460 (2004) 2381–2394.

[13] T. L. David, Chaotic behavior of reaction systems: mixed cubic and quadratic autocatalysis, Chemical Engineering Science 47 (1992) 4435–4444.

[14] T. L. David, Chaotic behavior of reaction systems: consecutive quadratic/cubic autocatalysis via intermedites, Chemical Engineering Science 48 (1993) 2103–2108.

[15] R. A. Satnoianu, P. K. Maini, M. Menzinger, Parameter space analysis, pattern sensitivity and model comparison for turing and stationary flow-distributed waves, Physica D 160 (2001) 79–102.

[16] Y. Tang, J. Wang, Bifurcation analysis on a reactor model with combination of quadratic and cubic steps, J. Math. Chem. 46 (2009) 1394–1408.

[17] B. G. Gray, M. J. Roberts, A method for the complete qualitative analysis of two coupled ordinary differential equations dependent on three parameters, Proc. Roy. Soc. Lond A 416 (1988) 361–389.

[18] V. Balakotaiah, D. Luss, Multiplicity features of reacting systems, Chem. Engng. Sci. 38 (1983) 1709–1721.

[19] J. Guckenheimer, P. Holmes, Nonlinear oscillations, dynamical systems, and bifurcations of vectorfields, Springer-Verlag, New York, 1983.

[20] M. Golubitsky, D. G. Schaeffer, Singularites and groups in bifurcation theory, Springer-Verlag, New York, 1985.